

CHARACTERIZATION OF PYROLYSIS OF NONG'AN OIL SHALE AT DIFFERENT TEMPERATURES AND ANALYSIS OF PYROLYSATE

JING HAN^(a,b), YOUHONG SUN^(a,b), WEI GUO^(a,b),
QIANG LI^(a,b), SUNHUA DENG^{(a,b)*}

^(a) College of Construction Engineering, Jilin University, Changchun 130021, PR China

^(b) National-Local Joint Engineering Laboratory of In-situ Conversion, Drilling and Exploitation Technology for Oil Shale, Changchun, Jilin, 130021, PR China

Abstract. *In this work, the thermal behavior of Nong'an oil shale of China was investigated and its pyrolysate analyzed in order to provide optimal pyrolysis parameters for the oil shale in-situ pyrolysis pilot project. Through thermogravimetric analysis (TGA) it was noted that the main mass loss of oil shale was in the temperature range of 310–600 °C and the maximum mass loss temperature was 465 °C. The retorting experiments showed that temperature had an important influence on shale oil yield and the maximum oil yield was obtained at 550 °C. The oil yield was reduced at higher temperatures, resulting in an increase in gas yield. According to the analysis of shale oil composition the high pyrolysis temperature could promote the formation of short-chain hydrocarbons. Meanwhile, more alkenes and aromatics and less heteroatomic compounds were found at high temperature. The long-chain hydrocarbons and heteroatomic compounds were proved to be secondary products decomposed at higher temperature. In addition, the results of nitrogen adsorption/desorption and scanning electron microscopy (SEM) indicated that the shale surface became more porous due to the decomposition of kerogen and more micro- and mesopores were found after the treatment at high temperature.*

Keywords: *Nong'an oil shale, pyrolysis process, shale oil, heating temperature.*

1. Introduction

With the rapid development of the world economy, energy demand is growing quickly. Oil shale, as an alternative source of energy, is a fine-grained sedimentary rock containing organic matter which is distributed in the framework of inorganic mineral. The countries that use oil shale refining are

* Corresponding author: e-mail denghua13@163.com

mainly China, Estonia and Brazil. China's oil shale resources are abundant, proven reserves converted into shale oil are about 133 billion tons [1] and are mainly distributed in the country's eastern regions, in the Songliao Basin, the Huadian Basin and the Fushun Basin. The Songliao Basin is a large Mesozoic oil-gas-bearing rift basin located on the Paleozoic suture basement of North China, Siberia and Jiamusi Massif [2, 3]. It contains abundant oil, gas and oil shale resources [4, 5]. The Nenjiang and Qingshankou Formations of the Upper Cretaceous are the main source rocks in the Songliao Basin [6]. The Nong'an region, which is located in the southeast uplift area of the southern Songliao Basin (Fig. 1), is one of the four large oil shale deposits discovered in China [1]. Nong'an oil shale is also developed in the Upper Cretaceous Qingshankou and Nenjiang Formations. Based on the National Cooperative Innovation Project on Chinese Potential Oil and Gas Resources, the resource evaluation in the Nong'an region was conducted, the identified oil shale reserves are especially abundant in the Nong'an mining area with a high potential for exploitation, while proven reserves are estimated at approximately 27.75 billion tons. However, the oil yield of Nong'an oil shale is low (4–5% on average), which will make the con-

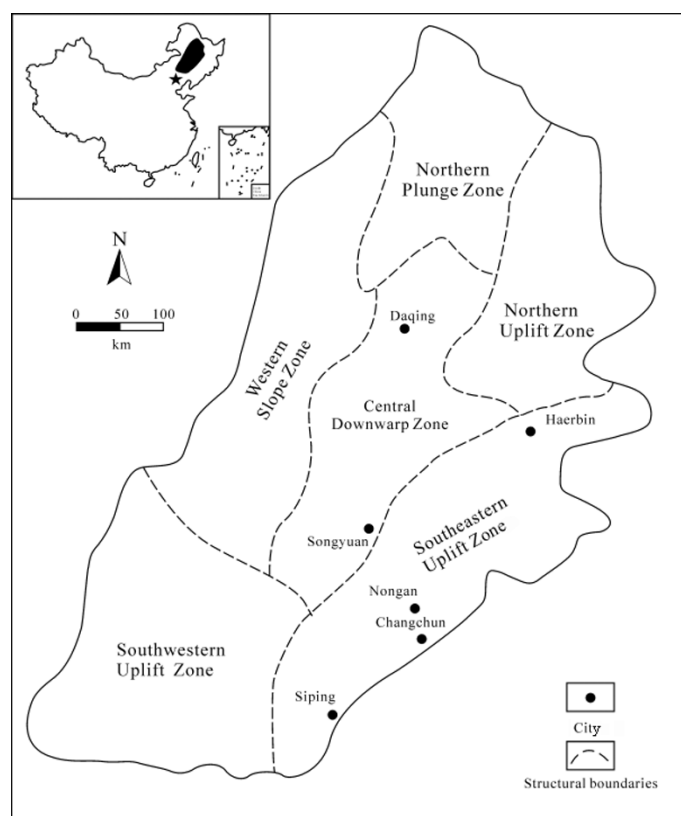


Fig. 1. Location of Nong'an oil shale (modified from [12]).

ventional development method too costly. Moreover, the surface above the oil shale resources is fertile farmland in the Nong'an region, so in-situ exploitation would be a suitable way to develop this kind of resource.

Many in-situ pyrolysis techniques have been proposed, including ICP (Shell) [7], ElectrofracTM (ExxonMobil) [8], AMSO (EGL) [9], in-situ convective heating process (Taiyuan University of Technology) [10], subcritical water extraction technology (Jilin University) [11], etc. Especially ICP and AMSO technologies have been applied to the in-situ pilot experiments. However, for the low-quality oil shale resources of the Songliao Basin, the ICP technology based on the heat conduction heating method is obviously not economic. Recently, the oil shale topochemical reaction method proposed by Jilin University has been investigated as a low-energy input method, which is characterized by the introduction of air during the pyrolysis process. Therefore, Jilin University has put forward the idea of in-situ development of Nong'an oil shale resources through this technology, and the pyrolysis characteristics of Nong'an oil shale will be the first to be clarified.

In numerous studies the pyrolysis characteristics of oil shale have been investigated, to determine optimal pyrolysis parameters, such as heating temperature and rate, pyrolysis atmosphere, particle size and mineral content. Thermogravimetric analysis (TGA) is widely used to find out mass loss with changing temperature in the dehydration and decomposition of organic matter. Jiang et al. [13] found that retorting temperature could obviously influence the shale oil yield in the study of Huadian oil shale. Kok [14] investigated the thermal behaviour of Seyitomer oil shale by using the thermogravimetry-differential scanning calorimetry (TG-DSC) method. The results showed that higher heating rates led to higher reaction temperature. Nazzal and Williams [15] studied the influence of temperature and steam on the products from the flash pyrolysis of Jordan oil shale and found that the presence of steam could improve the oil yield. Ahmad and Williams [16] reported that increasing the particle size resulted in the increase of oil yield. Gai et al. [17] indicated that pyrite could promote the conversion of oil shale. In addition to thermogravimetric analysis, methods such as gas chromatography-mass spectroscopy (GC-MS) [18], Fourier transform infrared spectroscopy (FTIR) [19, 20], nitrogen adsorption/desorption [21] and scanning electron microscopy (SEM) [22] were used to characterize the changes in pyrolysate composition and pore structure before and after pyrolysis of oil shale. Niu et al. [23] applied GC-MS to investigate the characteristics of shale oil, and finally provided reference for the design of experimental parameters. Tiwari et al. [24] pointed out that the evolution of pore structure was important for gas and liquid production and heat transfer. Sun et al. [25] analyzed the characteristics of Huadian oil shale products by using the topochemical method in combination with the above-mentioned methods.

However, so far, studies have mainly focused on high-quality oil shales, such as Huadian [26, 27] with an oil yield of 19%, Green River [20, 28] with a TOC content of 14%, Jordan [15, 29] with an average organic content between 9% and 13%, and Estonian oil shales containing a relatively high amount of hydrogen [30, 31] and some having the TOC content of up to 22% [32], while low-grade oil shales such as Nong'an have been dealt with very rarely. Although recent studies have revealed that oil shale in the Qingshankou Formation has a high TOC content [5, 33], the Nong'an area contains more low-quality oil shale resources. Research and utilization of low-oil-yield oil shale will further increase the development potential and value of the Nong'an mining area. Therefore, the relatively low-quality oil shale of the Nong'an area was selected for research in order to facilitate the comprehensive development and utilization of oil shale.

In this work, samples of Nong'an oil shale with a TOC value of 5.23% were used to explore its pyrolysis behavior and product distribution characteristics. The pyrolysis experiments were carried out at different temperatures in the open system. TGA, GC-MS, FTIR, nitrogen adsorption/desorption and SEM were employed to investigate the physical and chemical changes in oil shale during the thermal degradation. A comparison of the properties of products obtained at different temperatures was made using various combinations of the above methods. This work aims to study the influence of pyrolysis temperature on the thermal degradation of Nong'an oil shale. It is expected that the results will provide some references for further in-situ simulation experiments of Nong'an oil shale under formation pressure and high-pressure atmosphere.

2. Materials and methods

2.1. Material

The samples used in this study were taken from the planned pilot zone of the Nong'an area, Yongping Township, Nong'an County, Jilin Province, China (Fig. 1). In the pilot test area, Nong'an oil shale is mainly buried in shallow layers, and the depth of the target layer is evaluated to be between 63 and 73 m with the whole thickness of 54.4 m. Prior to the experiment, the sample was first pulverized and sieved to a grain size of 1–2 mm. The basic characteristics of Nong'an oil shale are presented in Table 1. The X-ray

Table 1. Physical properties of Nong'an oil shale

Ultimate analysis		Fischer assay analysis		Proximate analysis	
Component	Content, wt%	Component	Content, wt%	Component	Content, wt%
C	6.33	Shale oil	2.71	Moisture	4.22
H	1.37	Water	6.71	Volatile matter	12.94
N	0.50	Residue	87.68	Ash	82.99
S	1.10	Gas	2.90	Fixed carbon	6.26

diffraction analysis (XRD) pattern of raw oil shale is depicted in Figure 2. As can be seen from the figure, quartz is the main mineral in Nong'an oil shale. Carbonate, clay minerals and pyrite are also present in different proportions.

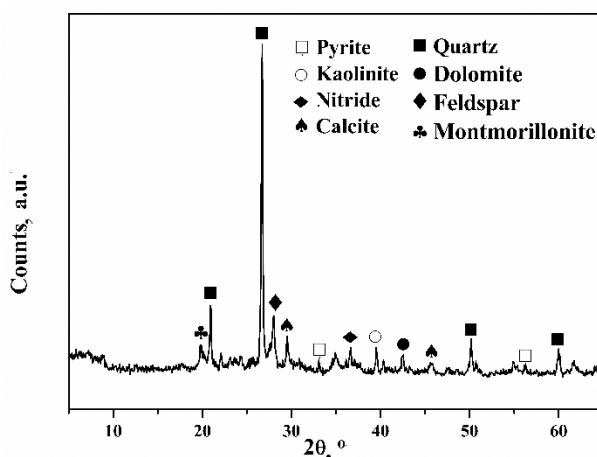


Fig. 2. XRD spectra of raw Nong'an oil shale.

2.2. Experimental apparatus and analysis methods

The schematic diagram of the experimental apparatus and analysis methods is shown in Figure 3. The pyrolysis experiments were carried out in a tube furnace under different temperatures (400–600 °C). During each experiment, 20.0 g of oil shale sample with a particle size of 1–2 mm was first placed in the middle of the tube furnace and plenty of nitrogen was introduced to remove the air. Then the tube furnace was heated to the specified temperature at 10 °C/min and held at said temperature for 2 hours to ensure the complete pyrolysis of oil shale. The gas sample was collected at 30 minutes after oil shale was heated to the specified temperature. The liquid collection device was placed in a constant temperature cold water bath to condense the generated oil and gas and water vapor. The residues were collected when the reactor was cooled to room temperature. The yields of shale oil, water, solid semi-coke and gas were calculated by the following formulas:

$$Y_o = \frac{M_l - V_w \rho_w}{M} \times 100\% , \quad (1)$$

$$Y_w = \frac{V_w \rho_w}{M} \times 100\% , \quad (2)$$

$$Y_s = \frac{M_s}{M} \times 100\% , \quad (3)$$

$$Y_g = 100\% - Y_o - Y_w - Y_s , \quad (4)$$

where Y_o , Y_w , Y_s and Y_g are the yields of shale oil, water, semi-coke and gas, respectively; M_l , M_s and M represent the masses of oil-water mixture, semi-coke and the original oil shale sample, respectively, V_w is the volume of water and ρ_w is the density of water. In order to ensure the accuracy of the experiment, each experiment was repeated at least 3 times under the same conditions, and the average oil yield was finally obtained.

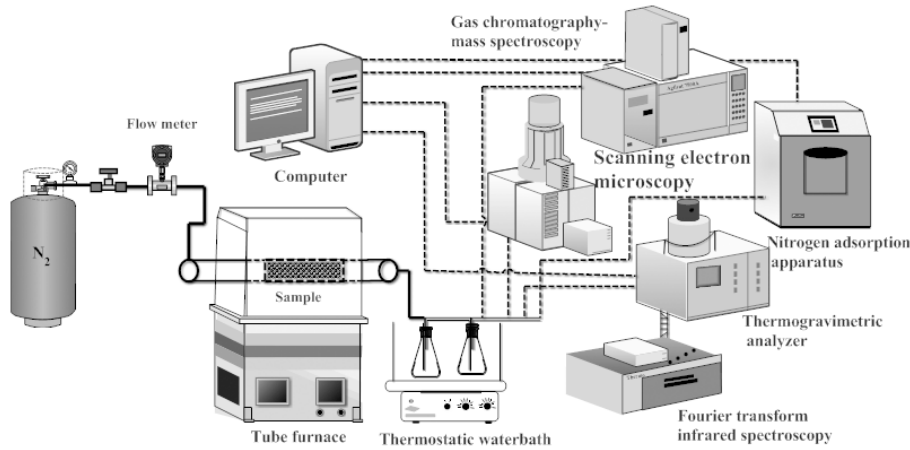


Fig. 3. The schematic diagram of experimental apparatus and analysis methods.

The TGA test was carried out using the Netzsch STA449F3 Synchronous Thermal Analyzer at a rate of 10 °C/min, in a high purity nitrogen atmosphere of 60 ml/min. The GC-MS test was performed using the Agilent 7890B-5975C gas chromatograph-mass spectrometer (USA). When the yield of shale oil was measured, the oven temperature was kept at 5 °C for 5 minutes and then raised to 280 °C at a rate of 10 °C/min followed by insulation for 12 minutes. In the shale gas yield measurement, the oven temperature was increased from 50 °C to 80 °C at a rate of 20 °C/min and then to 190 °C at 30 °C/min until the final temperature which was held for 9 minutes. The experiments were carried out several times to ensure reproducibility. The Agilent 7890A equipped with a thermal conductivity detector (TCD) and a flame ionization detector (FID) was used to identify the composition of the gas products. The oven temperature was kept at 40 °C for 2 minutes, and then increased to 150 °C at a rate of 20 °C/min until the final temperature hold for 13 minutes. FTIR was performed using the Nicolet iS10 FTIR Spectrometer (USA). The test sample was milled from about

1 mg of sample and 100 mg of dry KBr, then mixed evenly and compressed under a tablet press machine. The instrument used in the nitrogen adsorption and desorption experiments was the SSA-7000 specific surface area and pore size analyzer (China). The particle size of the sample used in the experiment was less than 100 μm , and the sample was degassed under vacuum at 180 $^{\circ}\text{C}$ for 3 hours before the nitrogen adsorption experiment. The surface porosity of raw oil shale and residues was investigated by SEM with the Hitachi S-4800 Field-emission Scanning Electron Microscope (Japan).

3. Results and discussion

3.1. The pyrolysis characteristics of raw oil shale and solid residues

Figure 4 shows the thermogravimetry (TG) and differential thermogravimetry (DTG) curves for Nong'an oil shale under N_2 atmosphere at a heating rate of 10 $^{\circ}\text{C}/\text{min}$. According to the quality change of oil shale, its pyrolysis is divided into three stages [34, 35]. In the first stage, the temperature rises from room temperature to 310 $^{\circ}\text{C}$, the small mass loss is mainly due to the evaporation of water, which mostly includes water and minerals in the clay mineral layer. The second stage is observed in a temperature range of 310–600 $^{\circ}\text{C}$, which is the main stage of oil and gas production. The mass loss is about 12.5%, which is due to the decomposition of organic matter in oil shale. The maximum mass loss temperature is 465 $^{\circ}\text{C}$, which provides the basis for choosing the retorting temperature for the subsequent pyrolysis experiment. When the temperature is higher than 600 $^{\circ}\text{C}$, the mass loss may be attributed to the pyrolysis of carbonate and clay minerals. In the third

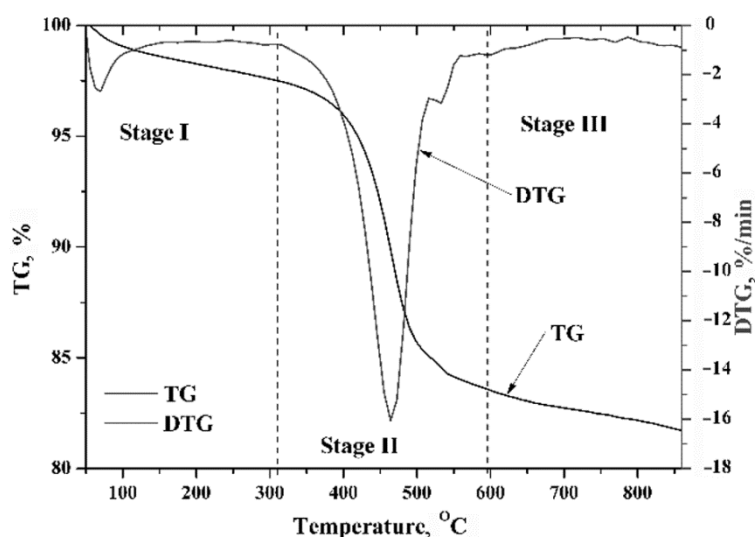


Fig. 4. TG and DTG results for raw Nong'an oil shale (heating rate: 10 $^{\circ}\text{C}/\text{min}$).

stage, the mass loss of Nong'an oil shale is much smaller, about 1.72%. It can be observed that the mass loss of oil shales from different areas, like Huadian oil shale, in the third stage of pyrolysis is different, because different oil shales contain different inorganic minerals and some of the minerals have a catalytic effect on the oil shale pyrolysis [36]. Based on the analysis of TG results, the retorting temperatures of 450, 500, 550 and 600 °C were selected for pyrolysis of Nong'an oil shale in order to determine the optimal final temperature. For convenience, raw Nong'an oil shale and residues are labeled S_{raw} , S_{450} , S_{500} , S_{550} , S_{600} . The subscript indicates raw oil shale or the specified temperature, i.e. S_{500} means the oil shale residue heated to 500 °C.

Table 2 gives the mass loss of raw Nong'an oil shale and solid residues. It can be seen that the mass loss of raw oil shale is 14.01%, but after heating treatment at 450 °C, the mass loss of the S_{450} sample is significantly reduced, indicating that most of the kerogen has been cracked at about 450 °C. But as the heating temperature increases, the mass loss in the second stage gradually decreases, and there is almost no mass loss of S_{600} , indicating that organic matter has been completely cracked.

Table 2. Mass loss of raw Nong'an oil shale and solid residues

Sample	Temperature interval, °C	Mass loss, %
S_{raw}	310–600	14.01
S_{450}	369–603	2.10
S_{500}	377–609	1.77
S_{550}	392–600	1.50
S_{600}	403–609	1.37

3.2. Influence of temperature on product distribution

The pyrolysis experiment of Nong'an oil shale was carried out based on the TGA results. Figure 5 shows the pyrolysate yields obtained at different anti-pyretic temperatures. It is clearly seen that the oil yield gradually increases with the rise of pyrolysis temperature and then decreases when the temperature increases to 600 °C. This is consistent with the organic matter cracking interval evidenced by the thermogravimetric results. At the same time, the yield of the residue gradually decreases. A similar phenomenon was also observed by Nazzal and Williams [15] when studying the pyrolysis of Jordan oil shale. A higher temperature can provide sufficient energy for cracking of kerogen and promote the production of oil and gas. At the same time, the yield of hydrocarbon gas increases with increasing pyrolysis temperature, which means that the high temperature is beneficial to production of more gas. In addition, the water yield is also increased at temperatures from 450 °C to 600 °C, which may be attributed to the decomposition of oxygen-containing heteroatomic compounds. Li et al. [37] also indicated that a lot of

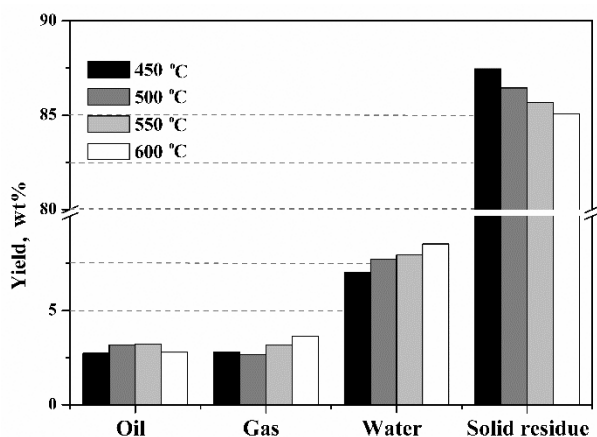


Fig. 5. Distribution of products obtained from the pyrolysis of Nong'an oil shale at different temperatures.

heteroatomic intermediates were formed in oil shale pyrolysis. These results show that an appropriate increase in temperature is advantageous to the complete pyrolysis of oil shale. For Nong'an oil shale, the retorting temperature between 500 °C and 550 °C is optimal to gain high oil yield.

3.3. Pyrolysis products of Nong'an oil shale

3.3.1. Shale oil

Figure 6 shows the GC-MS results for shale oil of Nong'an oil shale. It can be seen that the main components of shale oil are alkanes, alkenes, aromatic hydrocarbons and heteroatomic compounds, and alkanes and olefins appear in the bimodal form in the spectra. With the increase of pyrolysis temperature, it can be found that more short-chain hydrocarbons were generated. Jiang et al. [13] noted that in the pyrolysis process, a long-chain alkyl radical would be cracked into an olefin. This is more likely to happen at higher temperature.

Figure 7 shows the contents of the major components of the shale oil samples based on the normalization of the GC-MS peak area. With the heating temperature increasing from 450 °C to 600 °C, the area percentage of alkanes gradually drops from 73.58% to 53.60%, whereas that of alkenes and aromatic hydrocarbons increases from 15.84% to 27.33% and 1.32% to 5.85%, respectively. These results suggest that high temperature is favourable for production of more alkenes/alkanes, which agrees with the finding of Nazzal and Williams [15] in the study of flash pyrolysis of Jordan oil shale. Moreover, the amount of heteroatomic compounds in the pyrolysis intermediates decreases at temperatures from 500 °C to 600 °C. This implies that the heteroatom-containing fragments in the organic matter, especially

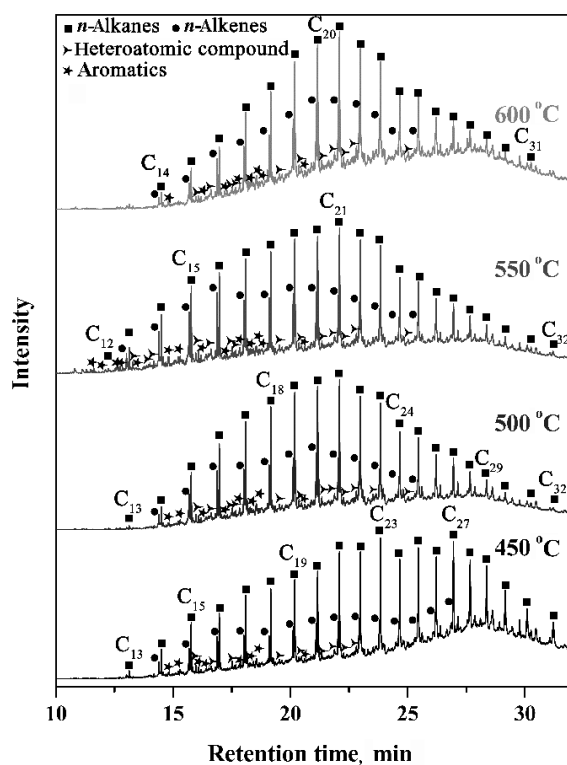


Fig. 6. GC-MS of shale oil from Nong'an oil shale obtained between 450 °C and 600 °C.

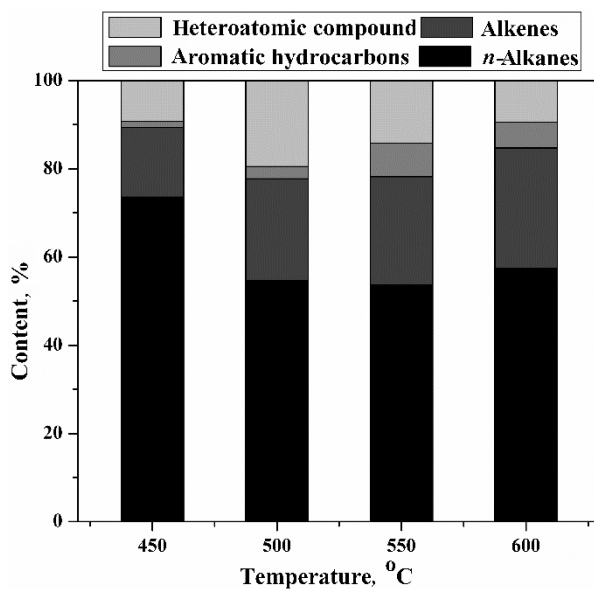


Fig. 7. Area percentage of shale oil components obtained between 450 °C and 600 °C based on GC-MS analysis.

oxygen-containing ones, are easily broken at a high temperature. This is another reason for the increase of olefins. At the same time, the removal of oxygen-containing groups also leads to the increase of water yield with increasing temperature.

3.3.2. Shale gas

The gas chromatograms of gases produced at different pyrolysis temperatures between 450 °C and 600 °C are shown in Figure 8. The organic gas species were relatively abundant at 450 °C. When the temperature reached 500 °C, 1-butene, 1-pentene and *n*-pentane began to decrease, because high temperature favours demethylation and the formation of methane. Above 500 °C, 1-butene, butane, *n*-pentene and pentane showed a decreasing trend as the pyrolysis temperature increased [23]. More short-chain hydrocarbons, especially methane, and less C^{3+} were found with the rise of pyrolysis temperature.

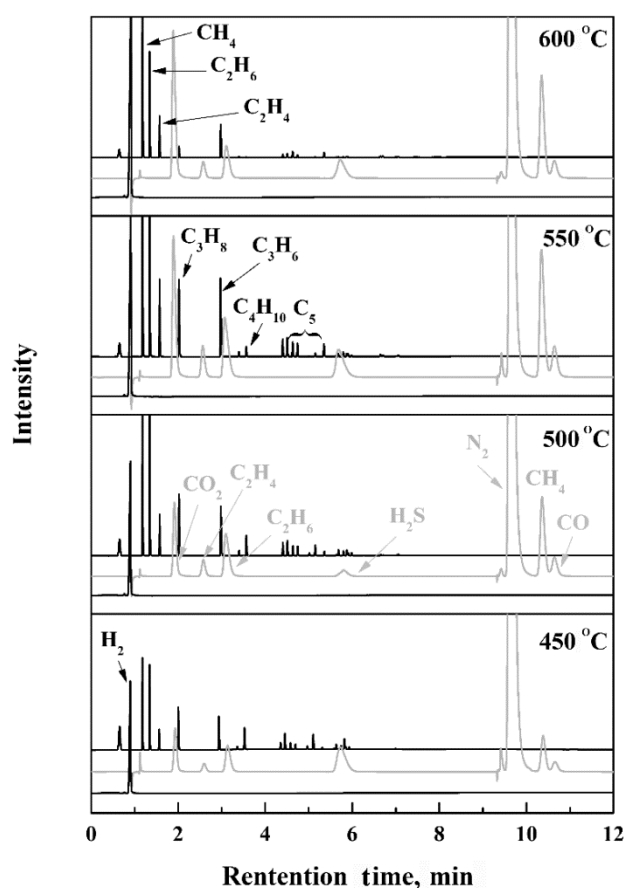


Fig. 8. GC spectra of shale gas obtained at different pyrolysis temperatures.

The emission curves of specific gaseous products are shown in Figure 9. As seen from the figure, the concentration of hydrogen increases at temperatures from 450 °C to 600 °C. This may be explained by that the dehydrogenation reaction is easy to occur at high temperature. H₂ originates from the condensation of free radicals, aromatic structures and hydrogenation of aromatic structures [25]. With rising temperature, the increase of CO₂ is partly attributed to the bonds in aliphatic and aromatic hydrocarbons, as well as to the breakage of oxygen-containing functional groups in oil shale, while some of the broken carbonyl species are precipitated in the form of CO and some are bound to oxygen atoms in oil shale [38]. When the temperature is further increased, carbon dioxide reacts with fixed carbon to produce carbon monoxide. This may be the reason for the reduction of carbon dioxide. Meanwhile, methane, ethane and ethylene gradually increased with increasing temperature and reached a maximum at 550 °C, which is due to the cleavage of aliphatic and arene side chain methyl functional groups. The results show that high temperatures promote the production of short-chain hydrocarbons. When the temperature is higher than 600 °C, all components except hydrogen and carbon dioxide tend to decrease. This is caused by the formation of a large amount of hydrogen and carbon dioxide, resulting in the reduction in hydrocarbon content. In addition, more H₂S is produced at 450 °C and 550 °C, which corresponds to the emission of organic sulfur and the decomposition of pyrite, respectively [17, 39]. Maaten et al. [40] confirmed that sulfur exists in the organic and mineral parts of oil shale. Gai et al. [17] suggested that the release of H₂S at 515–540 °C was associated with the pyritic sulfur.

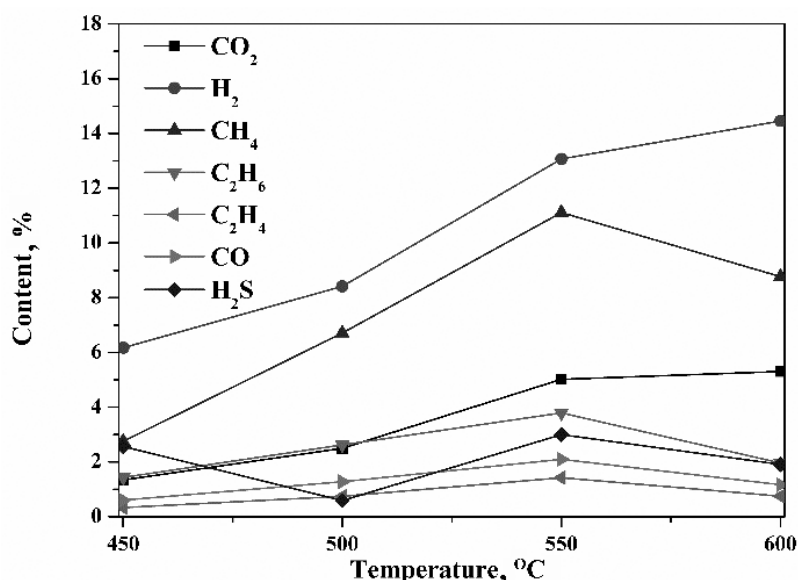


Fig. 9. Emission curves of specific gaseous products.

3.3.3. Solid residue

Figure 10 shows the FTIR spectra of raw Nong'an oil shale and solid residues treated at different temperatures. The functional groups displayed in these spectra can be used to determine the changes in the structure of oil shale during pyrolysis. Table 3 also gives the characteristic peaks of kerogen and inorganic minerals. The peaks at 2924 cm^{-1} , 2852 cm^{-1} and 1460 cm^{-1} belong to the C–H stretching bands of aliphatic compounds, asymmetric and symmetrical stretching vibrations and aromatic stretching vibrations of CH_2 , respectively. From Figure 10 and Table 3 it is obvious that the 2924 cm^{-1} , 2852 cm^{-1} and 1460 cm^{-1} peaks are attributable to the decrease of organics above $450\text{ }^\circ\text{C}$ and its complete disappearance at $550\text{ }^\circ\text{C}$, indicating that organic matter is not completely cracked at $450\text{ }^\circ\text{C}$. On the other hand, it is also indicated that some reactions occur only when the temperature is higher than $500\text{ }^\circ\text{C}$, which may also be the cause of the irregularity in the composition of oil obtained at $450\text{ }^\circ\text{C}$ and $500\text{ }^\circ\text{C}$. The peaks at 1089 cm^{-1} , 798 cm^{-1} and 778 cm^{-1} are mainly attributed to quartz, an important mineral component of oil shale. These results demonstrate that the chemical structure of oil shale is closely related to the pyrolysis temperature. This is also in accordance with the findings of Jia et al. [41]. Meanwhile, from the results of GC-MS and FTIR it can be deduced that there are obvious differences between pyrolysis reactions taking place at $450\text{ }^\circ\text{C}$ and $500\text{ }^\circ\text{C}$.

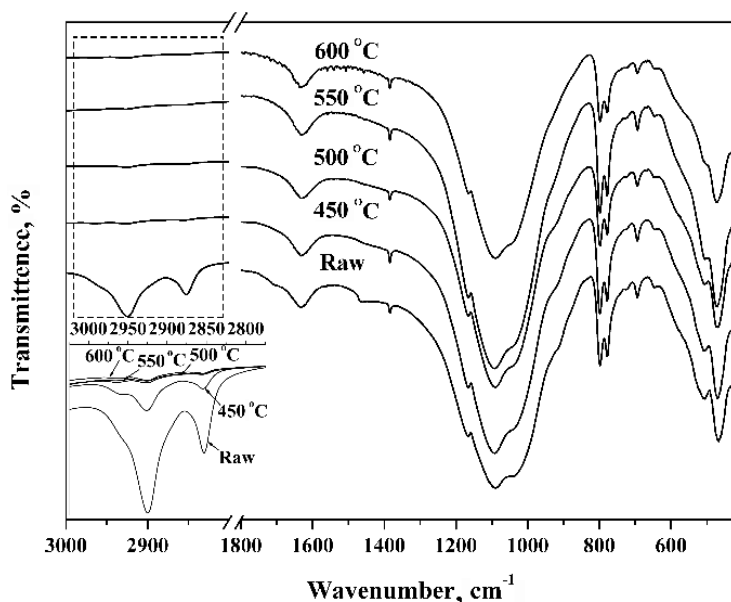


Fig. 10. FTIR spectra of raw Nong'an oil shale and solid residue treated at different temperatures.

Table 3. Major characteristic peaks in FTIR spectra of the main components of Nong'an oil shale

Wavenumber, cm^{-1}	Component
3630, 3430, 1631, 510, 470	Montmorillonite
2924, 2852, 1460, 1039	Kerogen
1089, 798, 778	Quartz
1164, 430	Pyrite
1870	Silicate
694	Calcite

Figure 11 shows the pore size distribution of the residue obtained as it is and at different temperatures. Although the change in the curve at 450–600 °C is not obvious, it can also reflect a certain trend. The micropores, especially of the size of 4 nm, gradually decrease as the pyrolysis temperature increases. 5–60 nm pores increase with increasing temperature, indicating that the pores are more developed during kerogen cracking.

Figure 12 depicts the variation of average pore volume and total specific surface area with temperature. Above 450 °C, the total specific surface area increases from 15.55 to 25.31 m^2/g and reaches a maximum at 500 °C, and then begins to decrease. The pore volume increases from 0.083 to 0.147 cm^3/g , and begins to decrease after reaching a maximum at 550 °C. This result is consistent with the conclusions of Bai et al. [42] and Wang and Cao [43].

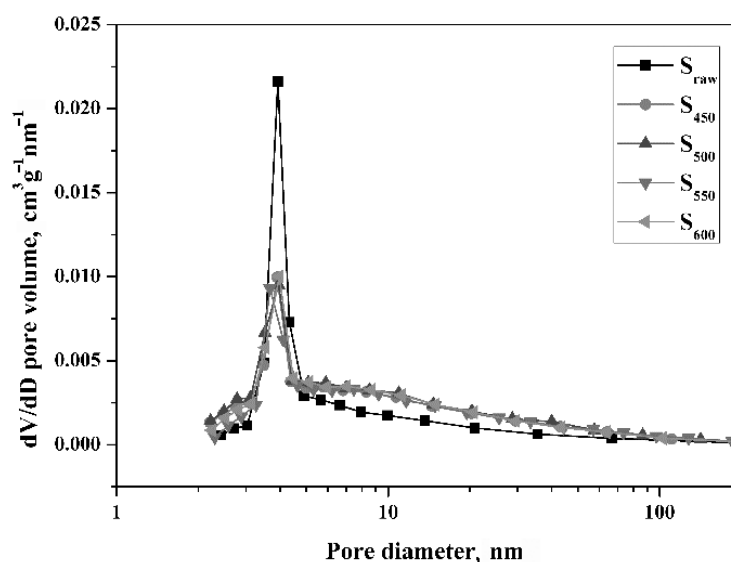


Fig. 11. Pore size distribution of oil shale and solid residue.

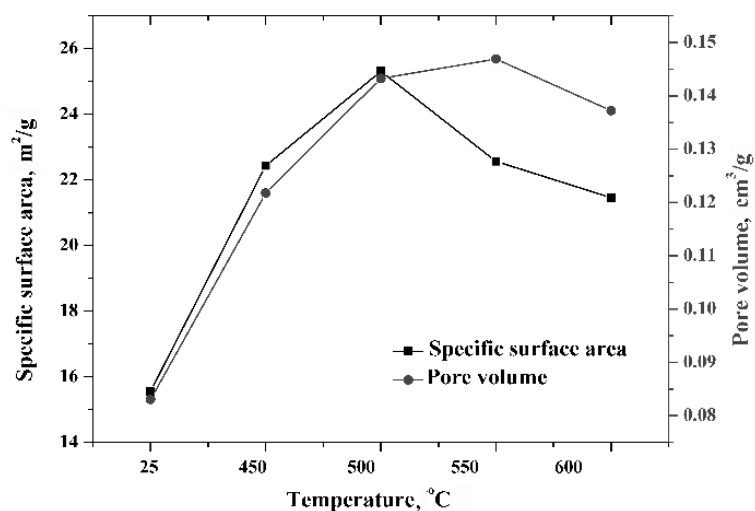


Fig. 12. Evolution of average pore volume and total BET specific surface area of oil shale and solid residue.

Scanning electron microscopy is mainly used to characterize the macropores which contribute less to the specific surface area. Figure 13 displays the SEM images of raw Nong'an oil shale and solid residues treated at different temperatures. Nong'an oil shale has typically characteristics of laminary sedimentary rocks which are possibly clay mineral aggregates, and some natural pores can be found on the surface (Fig. 13a). When treated at 450 °C, kerogen is cracked with the release of shale gas and oil, resulting in

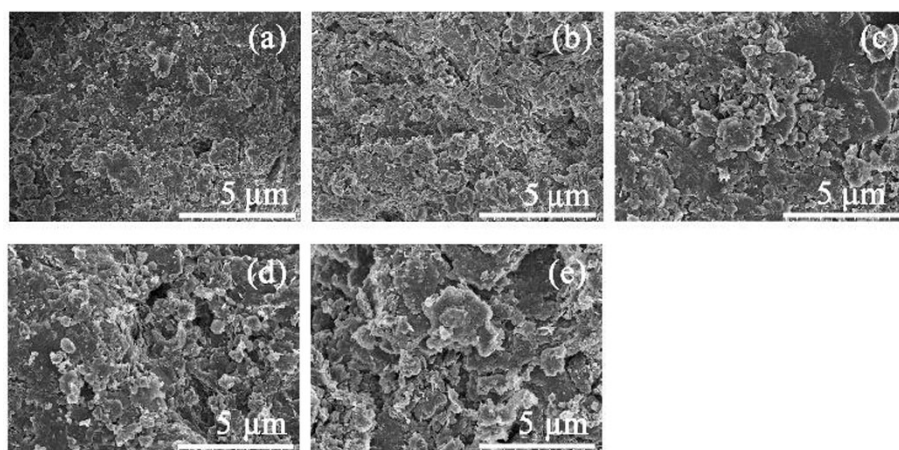


Fig. 13. SEM photographs of raw Nong'an oil shale and solid residues treated at different temperatures: a) S_{raw} , b) S_{450} , c) S_{500} , d) S_{550} , e) S_{600} .

the formation of tearing holes [25]. The shale surface becomes porous in the decomposition of kerogen during pyrolysis, being more obvious with the rise of temperature. Plenty of macropores within the sample are obviously developed due to the decomposition of organic matter and the collapse and coalescence of adjacent micro- and mesopores, which may lead to the increase of the permeability of rock [42]. Bai et al. [44] and Tiwari et al. [24] investigated the pore structure and permeability of oil shale and indicated that the evolution of pore structure during the pyrolysis process was essential for the heat transfer, reactivity, and the flow of gas and oil, especially for the in-situ pyrolysis process of oil shale. In their study of coal, Cai et al. [45] established that macropores had a significant impact on gas flow. Therefore, it could be concluded that high temperature would favour the expansion of the reaction zone and promote the production of oil and gas.

4. Conclusions

In summary, various analytical methods, such as thermal analysis technologies, gas chromatography-mass spectroscopy, Fourier transform-infrared spectroscopy, N₂ adsorption/desorption, and scanning electron microscopy, were employed to analyze the pyrolysis properties and pyrolysate of Nong'an oil shale. The decomposition temperature of the organic matter in Nong'an oil shale is 310–600 °C and the maximum mass loss temperature is 465 °C. The optimal heating temperature should be 500–550 °C. Higher temperatures promote kerogen cracking and increase shale oil yield, but when the temperature is higher than 550 °C, the yield of shale oil begins to decrease due to the production of a high amount of gas. In addition, the content of alkanes gradually decreases whereas that of alkenes and aromatic hydrocarbons increases with the rise of temperature. There are obvious differences between pyrolysis reactions at the heating temperatures of 450 °C and 500 °C. Some reactions may occur when the temperature is above 450 °C. The long-chain hydrocarbons and heteroatomic compounds decompose primarily at higher temperature. The demethylation and dehydrogenation reactions take place more easily with increasing temperature. Moreover, as the pyrolysis temperature increases, the specific surface area and pore volume of micro- and mesopores gradually increase at temperatures up to 550 °C. Meanwhile, the macropores increase with increasing temperature, which may promote the cracking of organic matter and provide a channel for the spillage of oil and gas products. The development of the pore structure is very important for the migration of oil and gas in oil shale in the in-situ pyrolysis process and can also affect the diffusion of the reaction zone. Therefore, the optimal pyrolysis temperature of Nong'an oil shale might be 550 °C for either high oil yield or oil migration.

The pyrolysis experiment in this study was carried out only in the open system. For the in-situ development pilot test, the pyrolysis experiment

under the conditions of formation pressure will be more instructive in the future.

Acknowledgements

This work was supported by the Project of Jilin Province Development and Reform Commission of China, the Cooperative Project between Universities and Jilin Province, China (Grant no. 274 SF2017-5-1), the Program for JLU Science and Technology Innovative Research Team (Grant no. 275 2017TD-13), the Fundamental Research Funds for the Central Universities, and the National Natural Science Foundation of China Youth Fund Project "Research in the subcritical water seepage behavior of in situ pyrolysis in oil shale (21406084)".

REFERENCES

1. Liu, Z., Meng, Q., Dong, Q., Zhu, J., Guo, W., Ye, S., Liu, R., Jia, J. Characteristics and resource potential of oil shale in China. *Oil Shale*, 2017, **34**(1), 15–41.
2. Feng, Z., Jia, C., Xie, X., Zhang, S., Feng, Z., Cross, T. Tectonostratigraphic units and stratigraphic sequences of the nonmarine Songliao basin, northeast China. *Basin Res.*, 2010, **22**(1), 79–95.
3. Wang, P., Mattern, F., Didenko, A., Zhu, D., Singer, B., Sun, X. Tectonics and cycle system of the Cretaceous Songliao Basin: An inverted active continental margin basin. *Earth-Sci. Rev.*, 2016, **159**, 82–102.
4. Bechtel, A., Jia, J., Strobl, S., Sachsenhofer, R., Liu, Z., Gratzer, R., Püttmann, W. Palaeoenvironmental conditions during deposition of the Upper Cretaceous oil shale sequences in the Songliao Basin (NE China): Implications from geochemical analysis. *Org. Geochem.*, 2012, **46**, 76–95.
5. Xu, J., Liu, Z., Bechtel, A., Meng, Q., Sun, P., Jia, J., Cheng, L., Song, Y. Basin evolution and oil shale deposition during Upper Cretaceous in the Songliao Basin (NE China): Implications from sequence stratigraphy and geochemistry. *Int. J. Coal Geol.*, 2015, **149**, 9–23.
6. Hu, F., Liu, Z., Meng, Q., Wang, J., Song, Q., Xie, W. Biomarker characterization of various oil shale grades in the Upper Cretaceous Qingshankou Formation, Southeastern Songliao Basin, NE China. *Oil Shale*, 2018, **35**(4), 304–326.
7. Brandt, A. R. Converting oil shale to liquid fuels: Energy inputs and greenhouse gas emissions of the Shell in situ conversion process. *Environ. Sci. Technol.*, 2008, **42**(19), 7489–7495.
8. Symington, W. A., Olgaard, D. L., Otten, G. A., Phillips, T. C., Thomas, M. M., Yeakel, J. D. ExxonMobil's Electrofrac process for in situ oil shale conversion. In: *Oil Shale: A Solution to the Liquid Fuel Dilemma. ACS Sym. Ser.*, 2010, **1032**, 185–216.
9. Burnham, A., Day, R., Wallman, P., McConaghy, J., Harris, H., Lerwick, P., Vawter, R. In situ method and system for extraction of oil from shale. *U.S. Patent 2011, 7,921,907*.

10. Yang, D., Elsworth, D., Kang, Z. Q., Zhao, Y. S., Zheng, B. Experiments on permeability evolution with temperature of oil shale. In: *Proceedings of the 46th US Rock Mechanics/Geomechanics Symposium*, Chicago, IL, USA, 24–27 June 2012, **3**, 1831–1835.
11. Deng, S., Wang, Z., Gao, Y., Gu, Q., Cui, X., Wang, H. Sub-critical water extraction of bitumen from Huadian oil shale lumps. *J. Anal. Appl. Pyrol.*, 2012, **98**, 151–158.
12. Cao, H., Kaufman, A. J., Shan, X., Cui, H., Zhang, G. Sulfur isotope constraints on marine transgression in the lacustrine Upper Cretaceous Songliao Basin, northeastern China. *Palaeogeogr. Palaeoclimatol.*, 2016, **451**, 152–163.
13. Jiang, H., Song, L., Cheng, Z., Chen, J., Zhang, L., Zhang, M., Hu, M., Li, J., Li, J. Influence of pyrolysis condition and transition metal salt on the product yield and characterization via Huadian oil shale pyrolysis. *J. Anal. Appl. Pyrol.*, 2015, **112**, 230–236.
14. Kok, M. V. Thermal investigation of Seyitomer oil shale. *Thermochim. Acta*, 2001, **369**(1–2), 149–155.
15. Nazzari, J. M., Williams, P. T. Influence of temperature and steam on the products from the flash pyrolysis of Jordan oil shale. *Int. J. Energ. Res.*, 2002, **26**(14), 1207–1219.
16. Ahmad, N., Williams, P. T. Influence of particle grain size on the yield and composition of products from the pyrolysis of oil shales. *J. Anal. Appl. Pyrol.*, 1998, **46**(1), 31–49.
17. Gai, R., Jin, L., Zhang, J., Wang, J., Hu, H. Effect of inherent and additional pyrite on the pyrolysis behavior of oil shale. *J. Anal. Appl. Pyrol.*, 2014, **105**, 342–347.
18. Lai, D., Shi, Y., Geng, S., Chen, Z., Gao, S., Zhan, J.-H., Xu, G. Secondary reactions in oil shale pyrolysis by solid heat carrier in a moving bed with internals. *Fuel*, 2016, **173**, 138–145.
19. Yuzbasi, N. S., Selçuk, N. Air and oxy-fuel combustion characteristics of biomass/lignite blends in TGA-FTIR. *Fuel Process. Technol.*, 2011, **92**(5), 1101–1108.
20. Le Doan, T. V., Bostrom, N. W., Burnham, A. K., Kleinberg, R. L., Pomerantz, A. E., Allix, P. Green River oil shale pyrolysis: semi-open conditions. *Energ. Fuel*, 2013, **27**(11), 6447–6459.
21. Han, H., Cao, Y., Chen, S.-j., Lu, J.-g., Huang, C.-x., Zhu, H.-h., Zhan, P., Gao, Y. Influence of particle size on gas-adsorption experiments of shales: An example from a Longmaxi Shale sample from the Sichuan Basin, China. *Fuel*, 2016, **186**, 750–757.
22. Josh, M., Esteban, L., Delle Piane, C., Sarout, J., Dewhurst, D. N., Clennell, M. B. Laboratory characterisation of shale properties. *J. Petrol. Sci. Eng.*, 2012, **88–89**, 107–124.
23. Niu, M., Wang, S., Han, X., Jiang, X. Yield and characteristics of shale oil from the retorting of oil shale and fine oil-shale ash mixtures. *Appl. Energ.*, 2013, **111**, 234–239.
24. Tiwari, P., Deo, M., Lin, C. L., Miller, J. D. Characterization of oil shale pore structure before and after pyrolysis by using X-ray micro CT. *Fuel*, 2013, **107**, 547–554.
25. Sun, Y., Bai, F., Liu, B., Liu, Y., Guo, M., Guo, W., Wang, Q., Lü, X., Yang, F., Yang, Y. Characterization of the oil shale products derived via topochemical reaction method. *Fuel*, 2014, **115**, 338–346.

26. Wang, S., Liu, J., Jiang, X., Han, X., Tong, J. Effect of heating rate on products yield and characteristics of non-condensable gases and shale oil obtained by retorting Dachengzi oil shale. *Oil Shale*, 2013, **30**(1), 27–47.
27. Wang, S., Jiang, X., Han, X., Tong, J. Effect of residence time on products yield and characteristics of shale oil and gases produced by low-temperature retorting of Dachengzi oil shale. *Oil Shale*, 2013, **30**(4), 501–516.
28. Bake, K. D., Pomerantz, A. E. Optical analysis of pyrolysis products of Green River oil shale. *Energ. Fuel.*, 2017, **31**(12), 13345–13352.
29. Jaber, J. O., Probert, S. D. Non-isothermal thermogravimetry and decomposition kinetics of two Jordanian oil shales under different processing conditions. *Fuel Process. Technol.*, 2000, **63**(1), 57–70.
30. Loo, L., Maaten, B., Neshumayev, D., Konist, A. Oxygen influence on Estonian kukersite oil shale devolatilization and char combustion. *Oil Shale*, 2017, **34**(3), 219–231.
31. Loo, L., Maaten, B., Siirde, A., Pihu, T., Konist, A. Experimental analysis of the combustion characteristics of Estonian oil shale in air and oxy-fuel atmospheres. *Fuel Process. Technol.*, 2015, **134**, 317–324.
32. Kosakowski, P., Kotarba, M. J., Piestrzyński, A., Shogenova, A., Więclaw, D. Petroleum source rock evaluation of the Alum and Dictyonema Shales (Upper Cambrian–Lower Ordovician) in the Baltic Basin and Podlasie Depression (eastern Poland). *Int. J. Earth Sci.*, 2016, **106**(2), 743–761.
33. Xu, J., Bechtel, A., Sachsenhofer, R. F., Liu, Z., Gratzner, R., Meng, Q., Song, Y. High resolution geochemical analysis of organic matter accumulation in the Qingshankou Formation, Upper Cretaceous, Songliao Basin (NE China). *Int. J. Coal Geol.*, 2015, **141–142**, 23–32.
34. Liu, Q., Han, X., Li, Q., Huang, Y., Jiang, X. TG–DSC analysis of pyrolysis process of two Chinese oil shales. *J. Therm. Anal. Calorim.*, 2013, **116**(1), 511–517.
35. Moine, E. c., Groune, K., El Hamidi, A., Khachani, M., Halim, M., Arsalane, S. Multistep process kinetics of the non-isothermal pyrolysis of Moroccan Rif oil shale. *Energy*, 2016, **115**, Part 1, 931–941.
36. Maaten, B., Loo, L., Konist, A., Siirde, A. Mineral matter effect on the decomposition of Ca-rich oil shale. *J. Therm. Anal. Calorim.*, 2018, **131**(3), 2087–2091.
37. Li, M., Zhan, J.-H., Lai, D., Tian, Y., Liu, X., Xu, G. Study on the evolution characteristic of intermediate during the pyrolysis of oil shale. *J. Therm. Anal. Calorim.*, 2017, **130**(3), 2227–2238.
38. Tiwari, P., Deo, M. Compositional and kinetic analysis of oil shale pyrolysis using TGA–MS. *Fuel*, 2012, **94**, 333–341.
39. Maaten, B., Loo, L., Konist, A., Pihu, T., Siirde, A. Investigation of the evolution of sulphur during the thermal degradation of different oil shales. *J. Anal. Appl. Pyrol.*, 2017, **128**, 405–411.
40. Maaten, B., Pikkor, H., Konist, A., Siirde, A. Determination of the total sulphur content of oil shale by using different analytical methods. *Oil Shale*, 2018, **35**(2), 144–153.
41. Jia, C., Wang, Z., Liu, H., Bai, J., Chi, M., Wang, Q. Pyrolysis behavior of Indonesia oil sand by TG-FTIR and in a fixed bed reactor. *J. Anal. Appl. Pyrol.*, 2015, **114**, 250–255.
42. Bai, F., Sun, Y., Liu, Y., Guo, M. Evaluation of the porous structure of Huadian oil shale during pyrolysis using multiple approaches. *Fuel*, 2017, **187**, 1–8.

43. Wang, L., Cao, H. Probable mechanism of organic pores evolution in shale: Case study in Dalong Formation, Lower Yangtze area, China. *J. Nat. Gas Geosci.*, 2016, **1**(4), 295–298.
44. Bai, J., Wang, Q., Jiao, G. Study on the pore structure of oil shale during low-temperature pyrolysis. *Energy Procedia*, 2012, **17**, Part B, 1689–1696.
45. Cai, Y., Liu, D., Pan, Z., Yao, Y., Li, J., Qiu, Y. Pore structure and its impact on CH₄ adsorption capacity and flow capability of bituminous and subbituminous coals from Northeast China. *Fuel*, 2013, **103**, 258–268.

Received January 18, 2019